

KINEMATICS OF 1200 KM/S JETS IN HE 3-1475

Kazimierz J. Borkowski

Department of Physics, North Carolina State University, Raleigh, NC 27695

`kborkow@unity.ncsu.edu`

and

J. Patrick Harrington

Department of Astronomy, University of Maryland, College Park, MD 20742

`jph@astro.umd.edu`

ABSTRACT

Spectroscopic observations of a proto-planetary nebula He 3-1475 with the Space Telescope Imaging Spectrograph (STIS) reveal the kinematics of its high (1200 km s^{-1}) velocity jets. The jets are formed at a large (0.15 pc) distance from its central star by collimation of an asymmetric stellar wind in a pair of conical shocks seen in Wide Field Planetary Camera (WFPC2) images. The jets consist of several pairs of knots symmetrically distributed with respect to the central star, with most knots exhibiting a head-tail morphology. Large (up to 650 km s^{-1}) radial velocity gradients are seen within the knots on subarcsec scales, with velocities decreasing from the knot heads toward their trailing tails. These large velocity gradients are a sign of efficient deceleration of jets by a much slower bipolar outflow. The inclination angle of the bipolar outflow is equal to 50° , based on Doppler shifts of the scattered stellar H α line. Its velocity is equal to 140 km s^{-1} at a distance of 0.23 pc from the star, and increases monotonically with the radial distance from the star. A comparison of new WFPC2 [N II] $\lambda 6584$ images with older WFPC2 images reveals expansion of the jets. The measured jet proper motions in combination with their radial velocities imply that He 3-1475 is a Galactic Bulge star at a distance of 8 kpc, located 800 pc above the Galactic plane. Its very high luminosity ($25,000 L_\odot$) implies that He 3-1475 must be significantly more massive than a typical AGB star within the Galactic Bulge, perhaps because of a past mass transfer and/or a merger event in a close binary system.

Subject headings: planetary nebulae: individual (He 3-1475) — ISM: jets and outflows — hydrodynamics — shock waves

1. INTRODUCTION

He 3-1475 is a B[e] type star located in the direction of the Galactic Bulge, at $l = 9^{\circ}4$, $b = +5^{\circ}8$. Stars of this spectral type do not show typical absorption line spectra, but instead numerous permitted and forbidden emission lines are superposed on featureless continua (for further information see a recent review on B[e] stars by Zickgraf 1998). He 3-1475 is an unusual B[e] star because it is surrounded by a dense expanding torus of circumstellar matter (CSM) seen in OH maser emission (Bobrowsky et al. 1995), and also as a prominent dark torus in Hubble Space Telescope (HST) images (Bobrowsky et al. 1995; Borkowski et al. 1997). A bipolar outflow and spectacular jets, perpendicular to the torus, were detected in the optical by Riera et al. (1995) and Bobrowsky et al. (1995). Radial velocities of bright knots in jets span 1000 km s^{-1} , which is an order of magnitude more than what is typically seen in both young and evolved stars surrounded by dense CSM. The morphology of the jets is also unusual, because they do not originate in the central star. Instead, a fast bipolar stellar outflow is apparently collimated far from the star in conical shocks seen in the HST images (Borkowski et al. 1997). The jets above the tips of conical shocks consist of a series of bright pairs of knots, located symmetrically with respect to the central star. Their spectra show the presence of substantial ($\sim 450 \text{ km s}^{-1}$) velocity gradients within the knots, which indicates their strong deceleration by the ambient, more slowly moving material in the bipolar lobes (Riera et al. 1995). There is also evidence for deceleration of knots on large scales, as the knot radial velocities decrease with increasing distance from the cone tips to the periphery of the bipolar outflow.

He 3-1475 is clearly an unusual source whose nature is not understood at present. Its distance has been estimated at $1 - 5 \text{ kpc}$ (Riera et al. 1995; Bobrowsky et al. 1995), which together with its high infrared flux (Parthasarathy & Pottasch 1989) suggests that He 3-1475 is probably a post-Asymptotic Giant Branch (AGB) proto-planetary nebula (PPN). (Knapp et al. 1995 detected 8.4 GHz continuum radio emission, which they interpreted as coming from a compact, newly formed PN close to the central star.) This conclusion should be considered preliminary because a reliable distance determination is lacking. The geometry of the circumstellar medium is also poorly known, with an uncertain (60° – Riera et al. 1995) inclination of the jets with respect to the plane of the sky. The velocity of the bipolar outflow and its age are unknown. This lack of fundamental knowledge about He 3-1475 makes it difficult to understand this puzzling object.

We report here on imaging and spectroscopic observations of He 3-1475 with the HST, which allow us to determine its distance, inclination and kinematics of its jets, and the velocity of the bipolar outflow. Imaging and astrometry with the Wide Field Planetary Camera (WFPC2) and the Space Telescope Imaging Spectrograph (STIS) data are presented and discussed in § 2 and § 3, respectively. The jet inclination and the distance to He 3-1475 are determined in § 4 and § 5, and the nature of He 3-1475 and of its jets are discussed in § 6.

2. WFPC2 IMAGING AND ASTROMETRY

The HST observed He 3-1475 on September 9, 1999, in a number of narrow-band WFPC2 filters, with the nebula located entirely on the Planetary Camera (PC) chip. We discuss here observations in the F658N filter encompassing the [N II] $\lambda 6584$ emission line, with the purpose of determining proper motion of brightest knots in the jets. Two pairs of images, shifted by 5.49 and 5.36 PC pixels along the horizontal and vertical axes, with each image 300 sec in duration, allows us to achieve nearly full HST spatial resolution. After standard HST pipeline calibration performed at the Space Telescope Science Institute, we reduced and analyzed the images with the Space Telescope Science Data Analysis Software. The “*crrej*” task was used to identify cosmic rays in each pair of images, resulting in creation of cosmic-ray “masks”. We then combined all 4 [N II] images using variable-pixel linear reconstruction (“drizzling”) as implemented in the “dither” package (Fruchter & Hook 1998). Briefly, with a Fourier cross correlation method (tasks “*crosscor*” and “*shiftfind*”), we aligned all images and then “drizzled” them with a “drop” size of 0.8 pixels onto a final image with 0.5 PC pixel size. In this procedure, we used the cosmic ray masks obtained previously from the “*crrej*” task. The final combined image (Figure 1a) has better spatial resolution and better signal-to-noise (S/N) ratio than the previous 600 sec [N II] image. Three pairs of prominent knots, the inner, middle, and outer pairs at approximate distances of 3'', 6'', and 8'' from the star, can be seen along the He 3-1475 jets. The inner pair of knots is located at or beyond the tips of conical shocks where the collimation of jets presumably takes place.

In order to determine the jet proper motion, we compared our new [N II] image with the previous HST [N II] image. This 1996 image consists of one pair of spatially coincident PC subimages, 400 sec and 200 sec in duration. We found the rotation angle of 31.683 degrees between the 1999 and 1996 images, again with the Fourier cross correlation method (task “*crosscor*” and “*rotfind*”), and then rotated and aligned the 1996 image with the 1999 image. The 1999-1996 [N II] difference image, corrected for the difference in exposure times, is shown in Figure 1b. This difference image clearly reveals the jet motion. Except for the bright inner region, where the artifacts from the imperfect subtraction of the central star dominate, all bright knots within the jet shifted outward from the star, as shown by a characteristic difference pattern with negative values closer to the star and with positive values on the outside. This radial motion is most prominent for the middle and inner pair of knots, although expansion is also seen for the blue-shifted outer knot. (The red-shifted outer knot is certainly also expanding, but this knot is affected by a bad PC column.) Motion of fainter knots and of individual features within the knots is also seen. For example, at least three features are seen moving outward in the brightest knot (the inner blue-shifted knot in the lower half of Figure 1), preceded on the outside by a bow-shock. Outward motion is also detected in the inner red-shifted jet, starting nearly at the base of the conical shock, and continuing along its knotty structure.

For quantitative measurements of proper motion, we chose the pair of bright middle knots. They are clearly more suitable for this purpose than fainter outer knots, and morphologies of these knots are considerably less complex than that of inner knots. There is also less contamination from

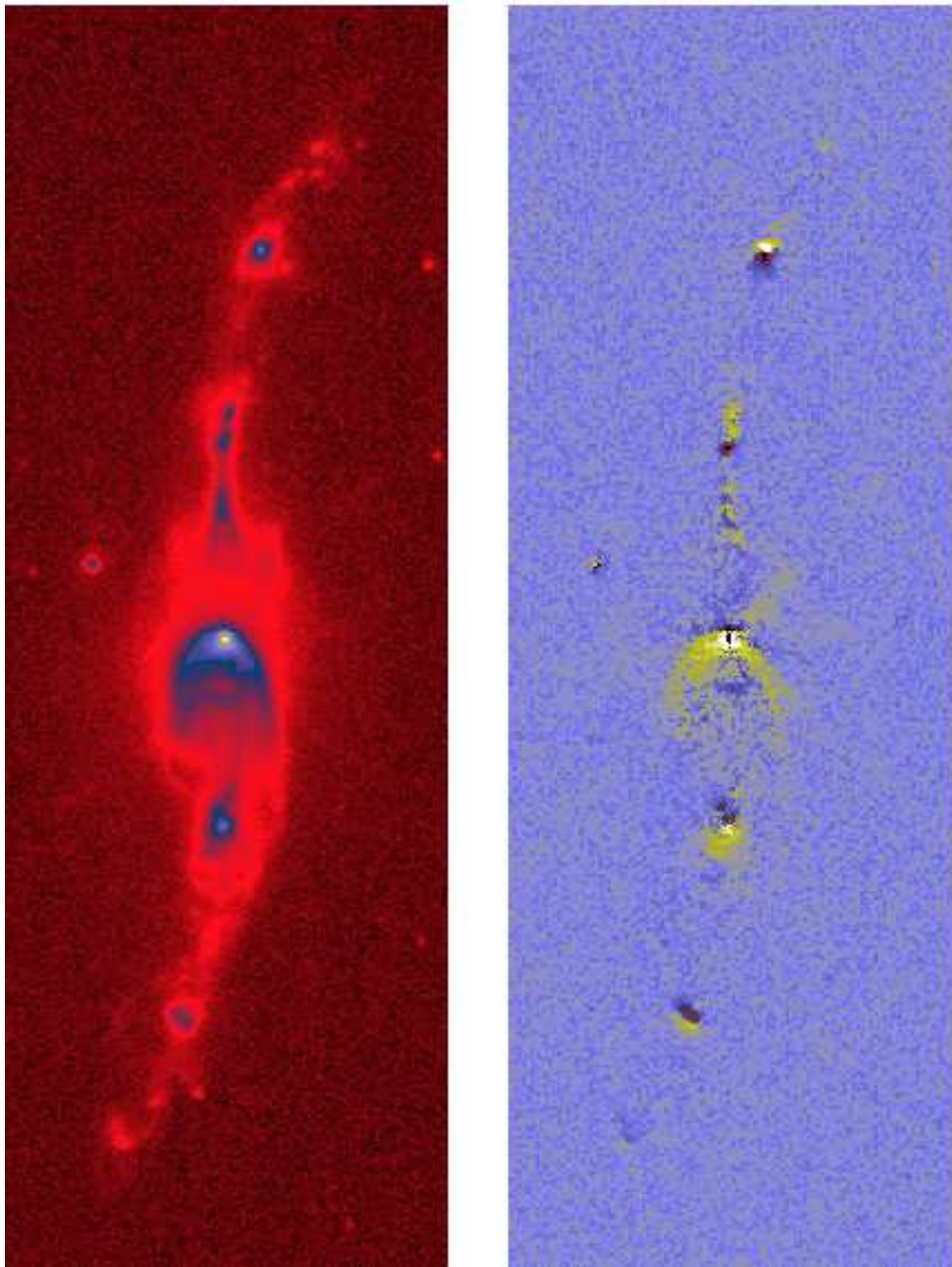


Fig. 1.— Protoplanetary nebula He 3-1475 imaged with the *Hubble Space Telescope* WFPC2 through the F658N ([N II] $\lambda 6584$) filter: a) the new 1200 sec image, b) the 1999-1996 difference image. Each image is $6''.8 \times 19''.3$ in size. The vertical axis is aligned with the STIS slits oriented at position angle of 135° (SE is at the top, NW at the bottom).

reflected stellar light at larger distances from the central star, which scatters from dense, more slowly moving material in the bipolar lobes of He 3-1475. We used a cross correlation technique to determine proper motions (Currie et al. 1996). Each pair of the 1999 images was combined with the “crrej” task to form two cosmic-ray cleaned images to be compared with the cosmic-ray cleaned 1996 image. We then chose image subsections encompassing each of the middle knots, and tapered their edges in order to avoid any edge effects. With the rotation angle determined as explained previously, we cross correlated these subimages, again using the Fourier technique as implemented in the “dither” package. For the central star, we found displacement between the images by fitting a two-dimensional Gaussian to the stellar image. The relative shifts between the knots and the central star were then averaged for the pair of 1999 images. We obtained radial shifts of 0.73 and 0.81 PC pixels, and tangential (counterclockwise) shifts of 0.00 and 0.12 pixels, for the middle red-shifted and blue-shifted knots, respectively. Statistical errors are just a few hundredths of a PC pixel, but real errors dominated by systematic effects are likely to be several times larger (Currie et al. 1996), maybe as large as 0.1–0.2 PC pixels. We also attempted to determine the displacement for the inner knots, arriving at radial displacements of 0.8 and 0.4 pixels for the brightest features in the red-shifted and the blue-shifted inner knots. These inner knots displacements are very uncertain because of the complex morphology of the inner knots and the presence of a more slowly moving material seen in the reflected stellar light. Additional difficulties may arise for a highly blue-shifted inner knot, where the [N II] emission falls on a rapidly changing F658 filter profile.

The radial displacements of the red-shifted and blue-shifted middle knots, 0.73 and 0.81 PC pixels (one PC pixel is equal to 45 miliarcsec), during the time interval of 3.24 years between the observations, imply proper motions of 10 and 11 miliarcsec yr^{-1} . The kinematic ages of these knots can be obtained by dividing their distances from the central star, equal to 5''.95 for the red-shifted knot and 5''.87 for the blue-shifted knot, by their proper motion. Their kinematic ages, 590 and 525 yr, are equal within the measurement errors, giving an average kinematic age of 550 yr for this pair of knots. This kinematic age should be considered as an upper limit to the actual age of the knots, because these knots were most likely formed at large distances from the central star, at the tips of conical shocks, and because of their continuing strong deceleration by a more slowly moving material in the bipolar lobes of He 3-1475.

3. JET KINEMATICS WITH STIS

Medium-resolution STIS spectra in the vicinity of $\text{H}\alpha$ were obtained on 15-16 June 1999. The G750M grating centered on 6581Å was used with the 0''.1 slit oriented along the jet axis. Spectra were obtained at nine parallel positions, with off-sets from the central star stepping from -0''.4 to 0''.4, so that the 5th position was centered on the star. To aid in removing cosmic ray hits, two exposures of about 20 min were taken at each position. In Figure 2 we show the spectrum in the vicinity of $\text{H}\alpha$ and [N II]. The second panel, Figure 2(W), is the WFPC2 image of the nebula on the same scale as the STIS spectra, while Figure 2(L) shows the sum of slits with displacements

of $-0''.4$, $-0''.3$, and $-0''.2$. Figure 2(R) shows displacements of $0''.2$, $0''.3$ and $0''.4$, while Figure 2(C) is from slits displaced $-0''.1$, $0''.0$, and $0''.1$. The vertical lines on the WFPC2 image mark the edges of these three slit groups. The logarithm of the intensity is shown to reveal the fainter features.

3.1. The Stellar Radial Velocity

From the central spectrum which includes the star, we have measured the radial velocities of the stellar Fe II $\lambda 6517.88$, $\lambda 6434.46$, $\lambda 6458.17$ and $\lambda 6371.22$ lines, as well as [O I] $\lambda 6302.045$ and $H\alpha$. From the first five, we obtain consistent values of $37.6 \pm 1.2 \text{ km s}^{-1}$. The central peak of $H\alpha$ yields 54.4 km s^{-1} , but this broad, asymmetric line is presumably formed in the optically thick stellar wind, with absorption eating into the blue side of the profile. The velocity of the Fe II lines is close to the centroid of the 1667 MHz OH maser emission, $+45 \text{ km s}^{-1}$ (Bobrowsky et al. 1995). Riera et al. (1995) deduced a higher systemic velocity of $+71 \text{ km s}^{-1}$ from the centroid of the jet emission. But since the jet velocities are $\sim 1000 \text{ km s}^{-1}$, a small fractional asymmetry in the jet outflow will degrade the accuracy of this approach. We adopt $+40 \text{ km s}^{-1}$ as the systemic radial velocity.

3.2. The Kinematics of the Gas

The first step in untangling the complex structure seen in Figure 2 is the realization that there are two sorts of features present: emission (presumably shock-excited) from the jets and knots, and reflected light from the central star. The emission is characterized by the presence of the $\lambda 6548$ and $\lambda 6583$ lines of [N II] flanking $H\alpha$ $\lambda 6563$. The reflected light features, on the other hand, are characterized by $H\alpha$ with a faint continuum, but without [N II], since the central star has a strong $H\alpha$ emission line (as well as many weaker emission lines of Fe II, etc.).

The most obvious features are the complex emission triplet seen in Figure 2(C). The upper section, above the central star, shows the red-shifted emission of the receding jet. The [N II] emission shows its maximum velocity of $\sim 945(905) \text{ km s}^{-1}$ where the conical shocks emerge from the shadow of the torus; the velocity then declines as we move to the cone tip and then to the pair of knots, dropping to $\sim 785(745) \text{ km s}^{-1}$ at the end. (The velocities in parenthesis are relative to the systemic velocity of 40 km s^{-1} .) All along the jet, however, we see a smear of emission from the maximum red-shift toward much lower velocities. This is especially pronounced beyond the cone tip at the knots. Clearly, all along the flow, material is being decelerated from velocities of $\sim 850(810) \text{ km s}^{-1}$ down to $\sim 200(160) \text{ km s}^{-1}$ within a very small spatial volume. Careful inspection shows that the “deceleration streaks” are not exactly horizontal: the lower velocity gas is a bit nearer the star. This is the head-tail structure referred to earlier. The effect is small: even where it is most noticeable (in the first knot beyond the cone tip of the receding jet) it only amounts to $\sim 0''.05$ (i.e., about one STIS pixel).

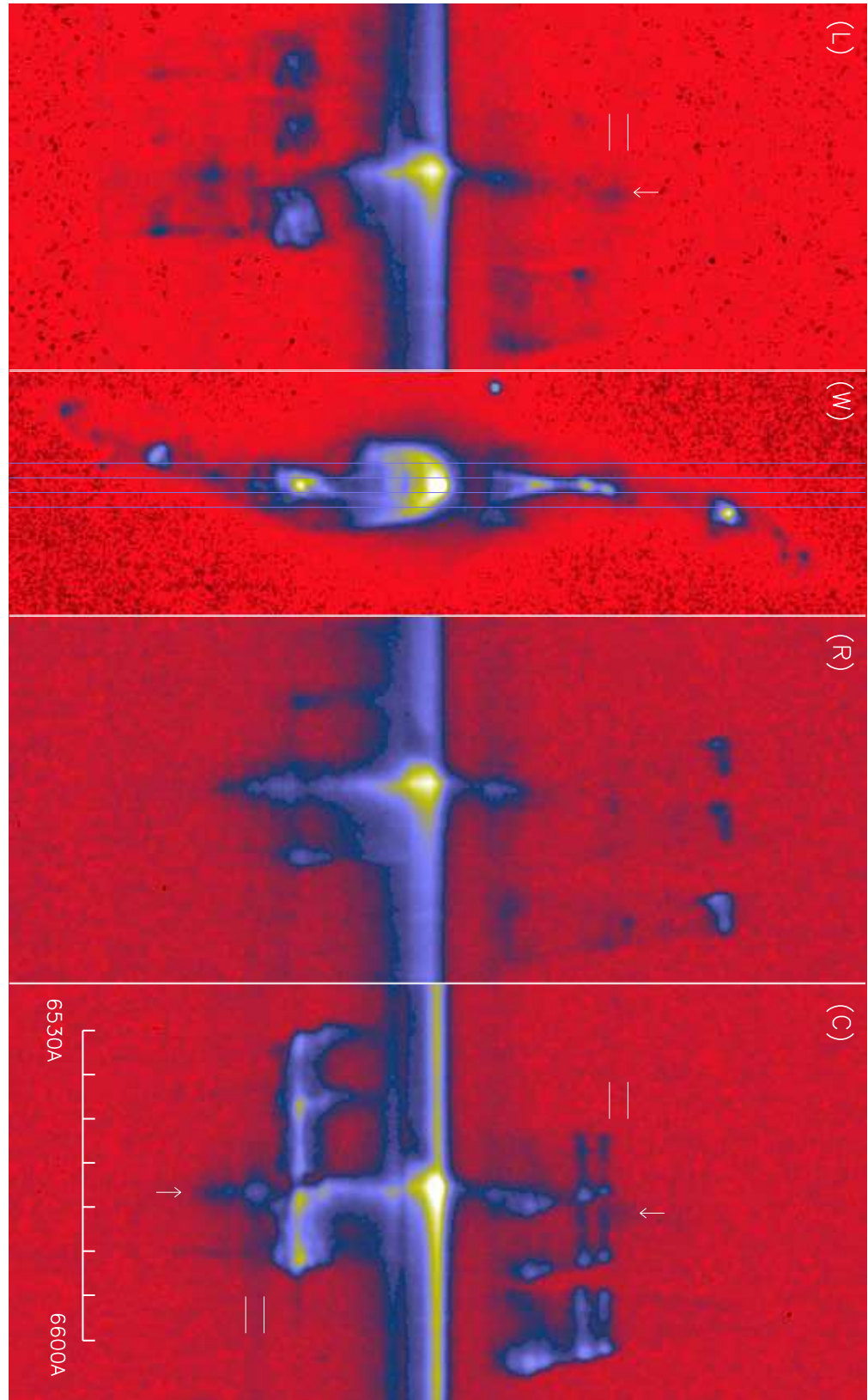


Fig. 2.— STIS spectra of He 3-1475 in the vicinity of H α . Panel (W) is the WFPC2 image through the F658N [N II] λ 6584 filter on the same spatial scale. Panels (L),(R) and (C) are extracted from the left, right and center regions, respectively, bounded by the vertical lines in panel (W).

Below the star, we see a corresponding pattern in the blue-shifted emission from the approaching jet. Here, there is some confusion because the reflected $\text{H}\alpha$ near the star blends with the blue-shifted $[\text{N II}] \lambda 6583$ line, but the $[\text{N II}] \lambda 6548$ and $\text{H}\alpha$ emission reveals what is happening. From where the emission first appears, it seems to increase in velocity slightly, reaching a maximum blue-shift of $\sim -910(-950)$ km s^{-1} just before the end of the conical structure. There is a small drop near the cone tip, but when the bright knot is encountered, a great smear of emission stretches from $\sim -795(-830)$ km s^{-1} down to $\sim -125(-165)$ km s^{-1} . Clearly, the knots are regions of violent deceleration. Closer examination, however, shows that the lower velocity emission is (faintly) present all along the jet. This suggests some sort of continuous turbulent interaction along a jet channel within a slower ambient gas.

Beyond the knot, we see an isolated line (marked by the arrow) – $\text{H}\alpha$ without any corresponding $[\text{N II}]$ emission, which indicates that this is starlight reflected from neutral, dusty gas. It is slightly red-shifted, an important point to which we will return in the next section.

Turning to Figure 2(R), we see that these slits miss the receding jet but do just graze the middle knot, where we see the emission triplet of $\text{H}\alpha$ and $[\text{N II}]$. The maximum red-shift out here is lower, $\sim 625(585)$ km s^{-1} . We see the same smear of emission down to $\sim 280(240)$ km s^{-1} . There is an interesting pattern here: if we take the maximum red-shift to represent the primary jet velocity, and the lowest red-shift to be related to the velocity of the ambient gas, then as we move away from the star, the jet velocity declines, while the velocity of the ambient gas increases. This inference is supported by the velocity pattern seen in reflection discussed in the next section.

Finally, Figure 2(L) shows the 3 slits which just touch the bright approaching knot. Unfortunately, the middle blue-shifted knot is beyond the last slit, though there is a bit of emission seen.

4. THE JET INCLINATION

Important information can be obtained by examining the Doppler shifts of the reflected stellar $\text{H}\alpha$ line. Consider the approaching jet. The reflected $\text{H}\alpha$ is marked by the lower arrow in Figure 2(C). We have extracted the spectrum from the brightest part, those rows between the horizontal lines, and this data is plotted as the triangles in Figure 3. The profile of the stellar $\text{H}\alpha$ emission line was taken from the slit passing through the star; using this stellar profile as a template with an adjustable amplitude and wavelength, we employed a Levenberg-Marquardt least-squares algorithm to produce the fit plotted as the solid line in Figure 3. Note that the reflected light has the same asymmetry as the stellar line. The result of this fit shows that the reflected light is red-shifted by $V_{\text{near}} = 32.4$ km s^{-1} (relative to the stellar feature). This velocity represents the difference between a red-shift of V due to the motion of the dust directly away from the star, and a blue-shift of $V \sin(i)$ due to the component of that motion directed towards us. Here, i is the inclination of the jet axis to the plane of the sky. On the other hand, light reflected from the receding jet will

show a larger red-shift: $V + V \sin(i)$. In Figure 2(C) and (L), the upper arrow marks the faint reflected H α line in the region just beyond the knot emission lines; the horizontal marks show the region we are discussing. Figure 2(L) shows the reflected line in the receding jet most clearly, since slits 1, 2 and 3 just miss the emission from the shock cone, resulting in less confusion. We have extracted the spectrum from the middle slit of the three which are combined in panel 2(L), the one with the $-0''.3$ offset, shown in Figure 4. The red-shift is clear in comparison with the unshifted stellar H α (the dashed line). The least squares fit (the solid line) found a red-shift $V_{far} = 248 \text{ km s}^{-1}$ relative to the stellar line. V_{far} and V_{near} were extracted at the same angular distance from the star, $3''.9$. Under the assumption that the velocity field of the dusty neutral gas is symmetric about the central star, so that the velocity V is the same for the far and near jets, we obtain a simple result for the inclination: $\sin(i) = (V_{far} - V_{near})/(V_{far} + V_{near})$. We thus determine the inclination to be 50° . The true velocity at this distance from the star is then $V = (V_{far} + V_{near})/2 = 140 \text{ km s}^{-1}$.

Though it becomes fainter, the reflected H α extends further from the star. It is clear that the red-shift on both sides increases with distance from the star. Fitting the stellar profile to the reflected line at an angular distance of $5''.3$, we find $V_{near} = 54 \text{ km s}^{-1}$ and $V_{far} = 353 \text{ km s}^{-1}$. This leads to nearly the same inclination, $i = 47^\circ$, and $V = 200 \text{ km s}^{-1}$. While we should give less weight to these values, the consistency of the inclination angle is reassuring. It also appears that the increase in V with distance from the star is approximately linear.

We can also obtain a limit on the inclination angle without relying on the assumed symmetry of the near and far jets. While the ionized gas which produces the emission lines spans a large range in velocity, the mechanism is one in which the fast-moving jet is decelerated by its interaction with the slower neutral gas. Thus the velocity of even the slowest ionized gas will be equal to or larger than the velocity of the neutral gas. (It need not be an equality since it is possible that the gas stops emitting [N II] line radiation when its velocity difference with the neutral gas drops below a certain value.) Thus we write $V_{ion}/V_{neut} = R \geq 1$, where V_{ion} and V_{neut} are the velocities, along the jet axis, of the slowest optically emitting gas and of the neutral gas, respectively. Then we find that

$$V_{neut} = V_{near} - V_{emiss}/R \quad \text{and} \quad \sin(i) = [1 + RV_{near}/(-V_{emiss})]^{-1}$$

where $V_{emiss} = V'_{emiss} - V_{star}$, the observed Doppler shift of the slowest emitting gas relative to the star. By setting $R = 1$ we find the maximum inclination angle. From the the [N II] emission just beyond the bright knot in the approaching jet, we find $V'_{emiss} = -150 \text{ km s}^{-1}$, so $V_{emiss} = -187 \text{ km s}^{-1}$. With $V_{near} = 32 \text{ km s}^{-1}$, the inclination is $i = 58.5^\circ$, and $V_{neut} = V_{ion} = 219 \text{ km s}^{-1}$.

Note, however, that an inclination of 58.5° implies a strong asymmetry in the jets: For the receding jet we require $V_{neut} = 134 \text{ km s}^{-1}$ to fit the observed V_{far} of the reflected H α line, which is 40% less than the velocity at the corresponding distance on the approaching side. Such a large difference seems in conflict with the overall symmetry we see in the emission line velocities of the near and far jets. On the other hand, with $R = 1.8$ we recover the symmetric solution, $i = 50^\circ$,

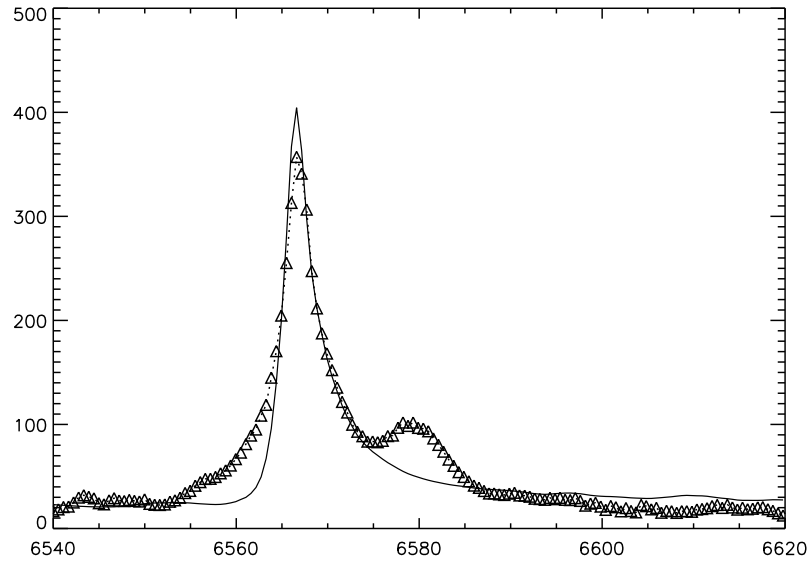


Fig. 3.— The stellar H α (solid line) fit to the reflected H α line (triangles) of the approaching jet.

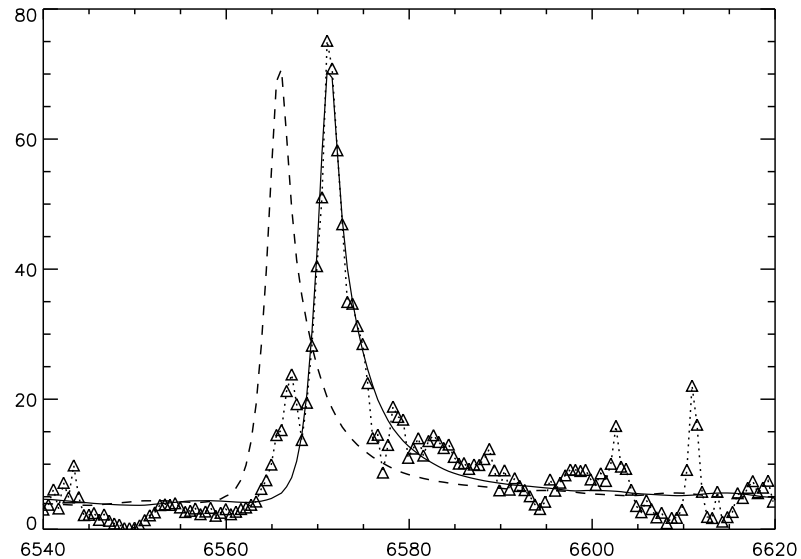


Fig. 4.— The stellar H α (solid line) fit to the reflected H α line (triangles) of the receding jet. The dashed line is the unshifted stellar profile.

with $V_{neut} = 137 \text{ km s}^{-1}$ and $V_{ion} = 244 \text{ km s}^{-1}$. We prefer this solution. If this interpretation is correct, then it follows that the jet flow stops emitting strongly when its velocity difference with the neutral gas drops below $\sim 100 \text{ km s}^{-1}$.

5. THE DISTANCE TO HE 3-1475

We may now find the distance to He 3-1475 by comparing the measured proper motions of the middle pair of knots with their tangential velocities. Our STIS spectra just graze the red-shifted knot (Fig. 2(R)), where we see emission line velocities between 240 and 585 km s^{-1} . Because the spectrum offset $0''.4$ shows higher velocities than that offset $0''.3$, and since no STIS spectra pass through the knot center, we likely underestimate the true knot velocities. In addition, we have no STIS spectra of the blue-shifted knot. We therefore use the ground-based radial velocities measured for the middle knots, v_r of $\pm 500 \text{ km s}^{-1}$ (Riera et al. 1995; Bobrowsky et al. 1995), to circumvent this problem. The implied tangential velocities v_T are $v_r / \tan 50^\circ = 420 \text{ km s}^{-1}$. Since we determined in § 2 that the average radial proper motion of the middle knots is $10.5 \text{ miliarcsec yr}^{-1}$, we arrive at a distance of 8.3 kpc. The galactic coordinates of He 3-1475 are $l = 9^\circ 4$ and $b = +5^\circ 8$, which in combination with the distance of 8.3 kpc implies that this star is located in the Galactic Bulge, 800 pc above the Galactic Plane.

We should note that we are making the assumption that our measured proper motions of the knot images correspond to the physical velocity of the emitting gas determined spectroscopically. That is, the knots are not just some sort of wave propagating along the jet. This seems plausible because the morphology of the middle knots is well defined and does not show any change between the epochs of observation. It would be useful, however, to observe the knots over a longer time interval. Detailed hydrodynamic modeling might also provide insights.

The velocity of the (neutral) bipolar outflow, as determined from the scattered stellar H α line, increases approximately linearly with the distance from the central star. We can then determine the kinematic age of this outflow from any knot within the bipolar outflow by dividing its projected distance from the central star by its tangential velocity. For example, the 140 km s^{-1} radial velocity of the brightest knot seen in the scattered light in the blue-shifted lobe (at distance of $3''.9$ from the star) translates into tangential velocity of 90 km s^{-1} . We then obtain an age of 1,700 yr at distance of 8.3 kpc. This age is several times longer than the age of the knots within the jet. We obtain a similar (1,300 yr) age for the material seen in the OH maser emission, assuming that the molecular outflow with a radial expansion velocity of 25 km s^{-1} and a spatial extent of $2''$ (Bobrowsky et al. 1995) is perpendicular to the jet. The bipolar outflow and the OH outflow apparently originated at the same time, perhaps at the time when the central star ejected the torus seen in the HST images, while the jet activity is more recent. This jet activity must be continuing now, as indicated by the short (120 yr) stellar wind travel time from the star to the cone tips.

6. DISCUSSION

Our distance determination places He 3-1475 in the Galactic Bulge, at a much larger distance than previously anticipated. At this distance its infrared luminosity is equal to 25,000 L_{\odot} (Riera et al. 1995), which might be less than the stellar luminosity if the dust optical depth is low along the bipolar outflow so that a substantial fraction of stellar luminosity escapes along the poles. He 3-1475 is apparently a high-luminosity Galactic Bulge star at a height of 800 pc above the Galactic plane. Its location suggests that He 3-1475 is an old Population II star, but an old, low-mass post-AGB star cannot be so luminous – a more massive star is required. Luminous, more massive AGB stars are indeed found in old stellar populations (e. g., in the globular cluster NGC 6553 – Guarnieri et al. 1997), although their luminosities may be several times lower than that of He 3-1475. It is also feasible that He 3-1475 is a member of a trace intermediate-age population of Galactic Bulge.

Irrespective of its age and origin, He 3-1475 appears to be an evolved star which lost a substantial amount of mass in a slow asymmetric wind at least 1,500 yr ago, possibly in a superwind at the AGB tip or during a binary interaction, and which is now seen in the optical as a dense torus. The presence of broad P-Cygni profiles in the stellar spectrum shows that the transition from the slow to the fast wind has occurred since then. The B[e] spectral classification of the central star implies that this fast wind is asymmetric, according to a disk wind model for B[e] stars by Zickgraf et al. (1985). This wind is perhaps driven by stellar UV radiation from a single fast rotating B type star (e. g., Pelupessy, Lamers, & Vink 2000), or more generally from a star + a disk system (Oudmaijer et al. 1998). This asymmetric wind is then collimated into 1200 km/s jets during its interaction with the more slowly moving material ejected earlier, maybe purely by hydrodynamical means (Borkowski et al. 1997). The time variability often seen in many B[e] stars suggests that a “knotty” jet morphology seen in He 3-1475 could be caused by temporal variations in the stellar wind properties.

Our STIS observations show how this high-velocity, time-dependent jet is decelerated by the circumstellar medium on both large and small scales. We see the large scale deceleration in the decrease of the maximum velocity as we move down the jet and out to the knots. But we also see at all points along the flow, and especially at the knots, local ($\sim 0''.05 = 6 \times 10^{15}$ cm) decelerations of over 500 km s⁻¹. Consider that a plane-parallel shock of 500 km s⁻¹ would produce gas with a temperature of 3×10^6 K, while we see a spectrum which seems more appropriate for a cooling shock of far lower velocity, about 100 km s⁻¹ (Riera et al. 1995). Clearly, there is much hydrodynamical structure which is still unresolved by HST.

It is still a mystery why B[e] star+disc systems are present in evolved post-AGB stars such as He 3-1475. There are a dozen such systems in compact PNe or proto-PNe (Lamers et al. 1998), albeit generally of lower luminosity than He 3-1475. The best known of these systems is the “Butterfly” PN M2-9, a low luminosity (550 L_{\odot}) object at a distance of 650 pc (Schwarz et al. 1997). M2-9 is clearly very much different than He 3-1475, suggesting that compact PN B[e] central

stars form a heterogeneous class, just like B[e] stars as a whole (Lamers et al. 1998). M2-9 shows a complex kinematics, with young (< 10 yr) micro-jets close to the star with velocities up to 195 km s^{-1} and much older (1,300 yr) bipolar outflows with velocities up to 140 km s^{-1} (Solf 2000). Doyle et al. (2000) find evidence for $\sim 1000 \text{ km s}^{-1}$ outflows. High velocity (500 km s^{-1}) outflows were also found by Redman et al. (2000) in another PN with a B[e] central star, Mz3, while spectacular jets were recently imaged by the HST in yet another PN on Lamers' et al. PN and PPN list, He 2-90 (Sahai & Nyman 2000). Both M2-9 and He 2-90 are suspected to be close binaries. A close binary progenitor hypothesis also seems attractive for He 3-1475, because its very high luminosity excludes a typical low-mass AGB star in the Galactic Bulge. A mass transfer binary and/or a merger event provides a reasonable solution to the presence of a more massive star in the Galactic Bulge.

We would like to thank Daniel Proga for stimulating discussions about the nature of B[e] stars. Support for this work was provided by NASA through grants GO-07285.01-96A and GO-07285.02-96A from the Space Telescope Science Institute, which is operated by the Association of Universities, Inc., under NASA contract NAS5-26555.

REFERENCES

Bobrowsky, M. et al. 1995, *ApJ*, 446, L89

Borkowski, K. J., Blondin, J. M., & Harrington, J. P. 1997, *ApJ*, 482, L97

Currie, D. G. et al. 1996, *AJ*, 112, 1115

Doyle, S., Balick, B., Corradi, R. L. M., & Schwarz, H. E. 2000, *AJ*, 119, 1339

Fruchter, A. S., & Hook, R. N. 1998, *astroph/9808087*

Guarnieri, M. D., Renzini, A., & Ortolani, S. 1997, *ApJ*, 477, L21

Knapp, G. R., Bowers, P. F., Young, K., & Philips, T. G. 1995, *ApJ*, 455, 293

Lamers, H. J. G. L. M., Zickgraf, F.-J., de Winter, D., Houziaux, L., & Zorec, J. 1998, *A&A*, 340, 117

Oudmaijer, R. D., Proga, D., Drew, J. E., & de Winter, D. 1998, *MNRAS*, 300, 170

Parthasarathy, M., & Pottasch, S. R. 1989, *A&A*, 225, 521

Pelupessy, I., Lamers, H. J. G. L. M., & Vink, J. S. 2000, *A&A*, 359, 695

Redman, M. P., O'Connor, J. A., Holloway, A. J., Bryce, M., & Meaburn, J. 2000, *MNRAS*, 312, L23

Riera, A., Garcia-Lario, P., Manchado, A., Pottasch, S. R., & Raga, A. C. 1995, A&A, 302, 137

Sahai, R., & Nyman, L.-Å. 2000, ApJ, 538, L145

Schwarz, H. E., Aspin, C., Corradi, R. L. M., & Reipurth, B. 1997, A&A, 319, 267

Solf, J. 2000, A&A, 354, 674

Zickgraf, F.-J. 1998, in B[e] Stars, eds. A. M. Hubert & C. Jaschek, (Kluwer: Dordrecht; Boston)

Zickgraf, F.-J., Wolf, B., Stahl, O., Leitherer, C., & Klare, G. 1985, A&A, 143, 421